Fast Events in Protein Folding: Structural Volume Changes Accompanying the Early Events in the N→I Transition of Apomyoglobin Induced by Ultrafast pH Jump

Stefania Abbruzzetti,*† Elisa Crema,* Laura Masino,* Arnaldo Vecli,*† Cristiano Viappiani,*† Jeanne R. Small,‡ Louis J. Libertini,§ and Enoch W. Small§

*Dipartimento di Fisica, Università di Parma, and †Istituto Nazionale per la Fisica della Materia, Parco area delle Scienze n. 7A, 43100 Parma, Italia; ‡Department of Chemistry and Biochemistry, Eastern Washington University, MS 74, Cheney, Washington USA; and §Quantum Northwest, Inc., Spokane, Washington USA

ABSTRACT Ultrafast, laser-induced pH jump with time-resolved photoacoustic detection has been used to investigate the early protonation steps leading to the formation of the compact acid intermediate (I) of apomyoglobin (ApoMb). When ApoMb is in its native state (N) at pH 7.0, rapid acidification induced by a laser pulse leads to two parallel protonation processes. One reaction can be attributed to the binding of protons to the imidazole rings of His24 and His119. Reaction with imidazole leads to an unusually large contraction of -82 ± 3 ml/mol, an enthalpy change of 8 ± 1 kcal/mol, and an apparent bimolecular rate constant of $(0.77 \pm 0.03) \times 10^{10}$ M^{-1} s^{-1}. Our experiments evidence a rate-limiting step for this process at high ApoMb concentrations, characterized by a value of $(0.60 \pm 0.07) \times 10^{6}$ s^{-1}. The second protonation reaction at pH 7.0 can be attributed to neutralization of carboxylate groups and is accompanied by an apparent expansion of 3.4 ± 0.2 ml/mol, occurring with an apparent bimolecular rate constant of $(1.25 \pm 0.02) \times 10^{11}$ M^{-1} s^{-1}, and a reaction enthalpy of about 2 kcal/mol. The activation energy for the processes associated with the protonation of His24 and His119 is 16.2 ± 0.9 kcal/mol, whereas that for the neutralization of carboxylates is 9.2 ± 0.9 kcal/mol. At pH 4.5 ApoMb is in a partially unfolded state (I) and rapid acidification experiments evidence only the process assigned to carboxylate protonation. The unusually large contraction and the high energetic barrier observed at pH 7.0 for the protonation of the His residues suggests that the formation of the compact acid intermediate involves a rate-limiting step after protonation.

INTRODUCTION

The mechanisms by which a protein folds to its native, functional state have not yet been resolved experimentally. In particular, the critical early stages leading from the disordered structure of the unfolded polypeptide to the native state are still poorly characterized.

A major impediment has been the limited time resolution of conventional rapid mixing techniques, which impose a limit of about 1 ms on the shortest observable times. Mixing-initiated refolding often leads to a fast, submillisecond burst phase during which much of the secondary structure is formed. The kinetic details of these nano- to microsecond changes are essentially inaccessible to traditional rapid mixing techniques, although some data have recently appeared on novel ultrarapid mixing methods with resolution reaching the tens of microseconds (Chan et al., 1997; Ramachandra Shastry et al., 1998).

Recently, modern laser T-jump instrumentation, coupled with various optical detection methods, has been applied to study the nanosecond-microsecond response of several model polypeptide systems (Williams et al., 1996; Thompson et al., 1997; Muñoz et al., 1997) and proteins (Phillips et al., 1995; Ballew et al., 1996b; Gilmanshin et al., 1997b, 1998) to a fast increase in the temperature. Using fluorescence emission of the N-terminal probe, 4-(methylamino)-benzoic acid, Thompson et al. (1997) characterized the kinetics of the helix-coil transition of a 21-residue alanine peptide. The thermally induced helix-coil transition in the same polypeptide was studied by Williams et al. (1996), who monitored the helix melting by infrared transient absorption in the amide I region. Temperature-induced unfolding of a hairpin was investigated by Muñoz et al. (1997) using fluorescence emission of the single tryptophan in the C-terminal fragment (41–56) of protein GB1. Other than model compound studies, few applications of laser T-jump techniques to proteins have been reported. Phillips et al. (1995) investigated the response of RNase A to a laser T-jump on the picosecond time scale by monitoring the infrared transient absorption in the amide I band. Thermally induced folding of apomyoglobin (ApoMb) has been studied by Ballew et al. (1996a,b) by monitoring the fluorescence emission of tryptophan and by Gilmanshin et al. (1997b, 1998) by measuring the amide I transient absorption. These studies evidenced complex kinetics with rates extending from tens of nanoseconds to hundreds of microseconds, involving different scale motions within the molecule.

Received for publication 16 March 1999 and in final form 8 October 1999.

Supported by National Institutes of Health grant R44 GM51147 (J. R. S., L. J. L., and E. W. S.). Instrumentation used in this work was developed, in part, using funds from National Science Foundation grant DMI-9522169.

Address reprint requests to Cristiano Viappiani, Dipartimento di Fisica, Università di Parma, Parco area delle Scienze n. 7A, 43100 Parma, Italia. Tel.: 39-0521905256; Fax: 39-0521905223; E-mail: cristiano.viappiani@fis.unipr.it.

0006-3495/00/01/405/11 $2.00

Ultrafast perturbations of protein stability can also be obtained by laser-induced pH jump, a methodology in which an aqueous solution containing a suitable photolabile caged compound (either proton or hydroxide) is flashed with a nanosecond UV laser (Gutman and Nachliel, 1990). In a series of works, Gutman and coworkers have investigated a number of proton transfer reactions, some involving biological macromolecules and supramolecular assemblies, using aromatic alcohols or heterosubstituted compounds and pulsed UV lasers to induce either a pH or a pOH jump. Although this technique was developed during the 1980s, no applications to the problem of protein folding have been reported so far.

In this work we have used a nanosecond UV laser and photolabile caged protons to perturb the native state of ApoMb, monitoring the structural response of the protein by means of time-resolved photoacoustics (Braslavsky and Heibel, 1992). We have recently applied this experimental methodology to follow proton transfer reactions in aqueous solutions, characterizing the solvation of photoinduced charges (Bonetti et al., 1997; Viappiani et al., 1998a; Small and Kurian, 1995; Losi and Viappiani, 1998), the formation of water molecules from proton and hydroxide (Viappiani et al., 1998a; Bonetti et al., 1997) and the reaction of protons with poly-L-lysine (Viappiani et al., 1998a). Proton transfer reactions induce large volume changes in the solution, due to strong electrostrictive effects and specific interactions with the solvent. Volume changes may be either positive (as for the neutralization of charged species) or negative (for ionization processes). When dealing with proteins, additional volume effects may result from structural changes of the macromolecules induced by protonation of amino acid residues. In the following we report the structural volume and enthalpy changes occurring on the nano- to microsecond time scale after perturbation of the native state of ApoMb with a nanosecond step increase in proton concentration. The measured parameters monitor early events for the acid-induced denaturation of native ApoMb.

Apomyoglobin, which is prepared by removing the heme group from myoglobin, contains eight strands of mostly α-helical segments, labeled A through H. According to the available NMR, CD, and calorimetric evidence, at neutral pH ApoMb adopts a native (N) structure that is similar to that of the native holomyoglobin (Hughson et al., 1990; Barrick and Baldwin, 1993; Cocco and Lecomte, 1994; Johnson and Walsh, 1994; Privalov, 1996). The ApoMb structure is characterized by a compact, hydrophobic core, consisting of at least the very stable A, G, and H helices, with roughly the same secondary structure content and tertiary fold as holomyoglobin. Although the A, G, and H helices form a distinct compact subdomain in the holoprotein, these helices isolated as separate fragments are unstable (Waltho et al., 1993; Hughson et al., 1991). At pH 4.0 the apoprotein adopts an equilibrium intermediate (I) conformation that has been the subject of numerous structural, thermodynamic, kinetic, and theoretical studies (Barrick et al., 1994; Privalov, 1996). This ApoMb intermediate shows a decreased helix content and lacks the tight side chain packing characteristic of globular protein cores (Hughson et al., 1991).

Extensive studies of the kinetics of ApoMb folding using conventional stopped flow initiation methods, SAXS, and hydrogen deuterium-pulsed labeling (Jennings and Wright, 1993; Eliezer et al., 1995) have revealed the rapid, submillisecond development of a compact acid intermediate in the kinetic folding pathway. Pulsed hydrogen-exchange experiments (Jennings and Wright, 1993) identified an early folding intermediate with a pattern of amide NH protection very similar to that seen for the equilibrium intermediate (Hughson et al., 1990), suggesting that the equilibrium intermediate is a kinetic folding intermediate.

We report here the first application of the laser pH jump technique with time-resolved photoacoustic detection to the ApoMb unfolding problem and, more generally, to the protein folding problem.

MATERIALS AND METHODS

Chemicals

Bromocresol purple (BP; Kodak) in water with 200 mM GuHCl was used as a calorimetric reference in all of the photoacoustic experiments. The pH of the reference solution was adjusted to 9.0, well above the pK_a of BP, in order to avoid instability in optical absorption at the excitation wavelength. *o*-Nitrobenzaldehyde (*o*NBA) was obtained from Sigma (St. Louis, MO) and was recrystallized from ethanol before use. Horse heart myoglobin was from Sigma.

Steady state absorption, far UV circular dichroism, and steady state fluorescence emission

Steady state absorption was measured with a Jasco 7850 UV-vis spectrophotometer. The steady state fluorescence emission (λ_{ex} = 295 nm) was measured with a Perkin-Elmer LS50 spectrofluorometer. The fluorescence emission was collected between 300 and 550 nm. Far UV circular dichroism was measured with a Jasco J700. All instruments were equipped with temperature-controlled sample holders.

Apomyoglobin preparation

Apomyoglobin was prepared by cold (−30°C) acid acetone extraction from horse heart myoglobin (Rossi Fanelli et al., 1958). The sample was washed with cold acetone and centrifuged several times, dried with pure nitrogen, and suspended in water containing GuHCl 200 mM at pH 7.0. GuHCl at 200 mM was used because it partially destabilizes the apoprotein and shifts the pK_a for the N→I transition toward neutrality (data not shown). The suspension was then centrifuged, and the supernatant was spectroscopically checked to assess sample purity. The concentration of the ApoMb stock was calculated from the absorption at 280 nm (ϵ = 15,800 $cm^{-1}M^{-1}$; Harrison and Blout, 1965) and heme contamination was estimated from the absorption at 408 nm (ϵ = 179,000 $cm^{-1}M^{-1}$; Harrison and Blout, 1965). In all the preparations, heme contamination was typically 0.5% of the total protein content.

Determination of the pK_a for the N→I transition

The pK_a of the N→I transition in the presence of GuHCl 200 mM at 1.8°C (*vide infra*) was determined by monitoring either the average helical content by circular dichroism (Barrick et al., 1994) or steady state tryptophan fluorescence emission (Ballew et al., 1996b). The results were then fitted to Eq. 1,

$$a = a_{\min} + (a_{\max} - a_{\min}) \frac{10^{n(pH-pK_a)}}{1 + 10^{n(pH-pK_a)}} \qquad (1)$$

which describes an ionic equilibrium monitored by the physically observable a (molar ellipticity per peptide residue, θ_{222}, or fluorescence intensity). The parameters a_{min} and a_{max} represent values observable at pH values far above and below pK_a, respectively. The parameter n represents an empirical Hill index ($n > 1$ positive cooperativity; $n < 1$ negative cooperativity; for $n = 1$, Eq. 1 reduces to the Henderson Hasselbalch equation). The value of n may also be interpreted as an estimate of the number of protons involved in the ionic equilibrium.

Fig. 1 reports changes in molar ellipticity per residue θ_{222} as a function of pH at 1.8°C, the temperature used for most of the experiments reported below. At pH 7.0, θ_{222} is 17,500 deg $dmol^{-1}$ cm^2, in agreement with previously reported values (Privalov, 1996; Barrick et al., 1994; Barrick and Baldwin, 1993). Fitting the data to Eq. 1, we estimated the pK_a for the formation of the compact acid intermediate in our experimental conditions as 5.85 ± 0.04, with a Hill index of 1.4 ± 0.2. The helical content of this intermediate is θ_{222} = 11,000 deg $dmol^{-1}$ cm^2, somewhat lower than reported by Barrick and coworkers (Barrick et al., 1994; Barrick and Baldwin, 1993) but more in line with the determination of Griko and Privalov (Privalov, 1996). The titration is fully reversible and no suggestion of aggregation was evident in any of our experiments.

The fluorescence of Trp14 is quenched when ApoMb is in state N at pH 7.0. Unfolding to the intermediate, I, results in increased fluorescence in response to the larger average distance between Trp14 on helix A and quenching groups on helix H. This quenching was initially attributed to interaction with Met131 (Ballew et al., 1996b), although recent data reported by Chen and Barkley show that Trp fluorescence emission is not quenched by Met (Chen and Barkley, 1998). Fig. 1 includes integrated fluorescence emission of apomyoglobin as a function of pH. From fitting Eq. 1 to the fluorescence data in Fig. 1, we obtained pK_a = 5.52 ± 0.03 and n = 1.9 ± 0.2. The pK_a for the N→I transition at T = 1.8°C obtained from fluorescence is slightly smaller than the result from far UV circular dichroism measurements. In contrast, at room temperature the pK_a and the index n are identical for both techniques (data not shown).

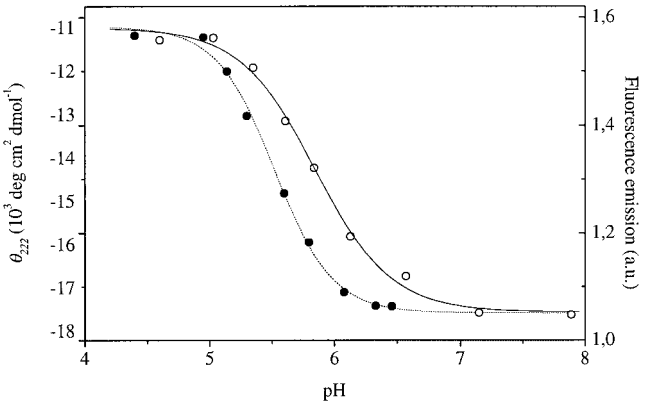

FIGURE 1 (○) Molar ellipticity per residue at 222 nm at various pH values of an aqueous solution of ApoMb at 1.8°C. [GuHCl] = 0.2 M, [ApoMb] = 15 μM. (●) Integrated fluorescence emission of an aqueous solution of ApoMb at 1.8°C. [GuHCl] = 0.2 M, [ApoMb] = 5 μM. λ_{ex} was 295 nm and the emission was collected between 300 and 550 nm.

Sample preparation for photoacoustics experiments

Solutions for photoacoustics measurements were prepared by diluting the concentrated ApoMb stock solution (in 200 mM GuHCl) into an aqueous solution containing 200 mM GuHCl and sufficient *o*NBA to give a final absorbance at 355 nm of 0.4 (1 cm path length). The concentration of CO_2 was reduced as much as possible by bubbling pure nitrogen through the solution for >30 min before addition of the ApoMb and then maintaining a nitrogen atmosphere until the measurements were completed. The pH was then adjusted by addition of concentrated HCl or NaOH and measured using a micro pH electrode immersed in the sample cuvette. The solutions were unbuffered beyond that contributed by the ApoMb (and the small amount of CO_2 that could not be removed from the concentrated ApoMb stock solution). Any added buffer would render the overall kinetics more complex due to competition for the photoreleased protons.

The photocalorimetric reference compound was dissolved in the same solvent as the sample. The thermoelastic parameter ($C_p\rho/\beta$) (*vide infra*) has been found to be independent of the protein concentration and the pH of the solution within the ranges employed in this work. The relatively high concentration of GuHCl present in both reference and sample solutions is mainly responsible for changing the thermoelastic properties of the solution from those of water. The value of ($\beta/C_p\rho$) of the solutions containing 200 mM GuHCl is positive above 1.79°C (*vide infra*) and becomes negative below this temperature.

The thermoelastic parameter ($C_p\rho/\beta$) of 200 mM GuHCl as a function of temperature was determined by using BP as a reference compound in pure water compared to 200 mM GuHCl (Braslavsky and Heibel, 1992).

Photoacoustic setup

Photoexcitation was achieved by the 355-nm third harmonic of a Q-switched Nd:YAG laser (Surelite II-10, Continuum). Part of the output was directed to an energy meter (Laser Precision RJ-7620) equipped with a pyroelectric energy probe (Laser Precision RjP-735) for normalization purposes. A smaller fraction was diverted to the sample and the unfocused beam was shaped by means of a slit 280 μm wide positioned in front of the quartz cuvette. The energy entering the sample was adjusted between 3 and 30 μJ using neutral density filters. No significant changes with laser fluence were observed in any of the measured parameters, except that the S/N ratio degraded at the lower energies.

In the experiments reported here, the photoacoustic pressure wave generated by laser pulse absorption was detected by a PZT piezoelectric transducer (Panametrics V-103). The signal was then amplified (60 db) and recorded by a digitizing oscilloscope (LeCroy 9450A) operated at 2.5 ns/channel. Typically 4000 time points were acquired, within a time window of 10 μs. The quartz sample cuvette was mounted in a temperature-controlled sample holder (TASC 300, Quantum Northwest, Spokane, WA), which assured a temperature stability of better than ±0.02°C inside the solution. The sample compartment includes magnetic stirring of the sample as well as a dry gas purge to prevent condensation of humidity on the cuvette walls at low temperatures. Dry nitrogen was used as the purge gas to minimize absorption of CO_2 during the experiment. Generally 100 waveforms were averaged for the reference signal, whereas only 9 waveforms were averaged for the samples to avoid extensive photodegradation of *o*NBA. Data acquisition and analysis were performed using dedicated software (Sound Acquisition and Sound Analysis, Quantum Northwest).

Analysis of photoacoustics data

The principles of deconvolution of photoacoustic waveforms have been described (Small et al., 1992; Small, 1992; Rudzki et al., 1985). In our case,

the system under investigation undergoes a mixture of parallel and sequential reactions characterized by well-separated rate constants and can be appropriately analyzed by a parallel decay model. The time derivative $H(t)$ of the overall time-dependent volume change is assumed to be a sum of single exponential decay functions:

$$H(t) = \sum_{i} \frac{\varphi_i}{\tau_i} e^{-(t/\tau_i)} \quad (2)$$

where φ_i is the pre-exponential factor of the transient with lifetime τ_i.

The experiments were repeated in triplicate and the parameters recovered (φ_i and τ_i) from deconvolution used to determine an average value and estimate the error bars.

The lower limit for time resolution of the experimental setup, afforded by the numerical deconvolution of the photoacoustic waveforms (Small, 1992), is about 20 ns, and the longest detectable lifetime is on the order of 10 μs.

We have determined the structural volume changes as a function of the solution pH and of the concentration of ApoMb using a two-temperature (TT) method (Gensch and Braslavsky, 1997). The sample waveform is acquired at the temperature $T_{\beta=0}$ for which the thermal expansion coefficient of the solution, β, is zero; in water this temperature is close to 3.9°C (Weast, 1971), whereas the reference waveform is measured at a slightly higher temperature $T_{\beta=0}$, close enough to $T_{\beta=0}$ so that the compressibility may be considered unchanged. The value of $T_{\beta=0}$ can be determined experimentally by measuring the temperature at which the signal for the reference compound, BP, vanishes. Under our experimental conditions (200 mM GuHCl) we found $T_{\beta=0}$ = 1.79°C. Signals measured at $T_{\beta=0}$ originate solely from structural volume changes in the solution and include no enthalpic contributions.

The extent of the observed structural volume change ΔV_i (estimated as milliliters per mole of absorbed photons) is calculated from φ_i as:

$$\Delta V_i = \varphi_i E_\lambda \left(\frac{\beta}{C_p \rho}\right)_{\beta \neq 0} \quad (3)$$

where E_λ is the energy of 1-mole photons at the excitation wavelength and $(\beta/C_p\rho)_{\beta\neq0}$ is the thermoelastic parameter of the solution at $T_{\beta\neq0}$. In order to express the volume changes as milliliters per mole of protons released we must divide ΔV_i by the deprotonation quantum yield, Φ_H^+ = 0.4, of *o*NBA (George and Scaiano, 1980).

Experiments conducted at multiple temperatures (MT method) have been used to determine for each transient the heat release, the structural volume change and, from temperature dependence of the rate constants, the activation energy (Callis et al., 1972; Peters and Snyder, 1988; Braslavsky and Heibel, 1992). Deconvolution was performed at several temperatures, and the pre-exponential factors φ_i were used to determine the energy content $E_\lambda\varphi_i$ of the transients at each temperature. This parameter was then plotted versus the thermoelastic parameter of the solution, $(C_p\rho/\beta)$. From the linear relation:

$$\varphi_i E_\lambda = Q_i + \Delta V_i \left(\frac{C_p \rho}{\beta}\right) \quad (4)$$

it is possible to determine the heat released Q_i (from the intercept) and the volume change $\Delta V_i = \Phi_i \Delta V_{R,i}$ (from the slope) for each of the transients, where Φ_i is the quantum yield of step *i*. If Φ_i is known, then it is possible to determine the molar reaction volume $\Delta V_{R,i}$ (expressed as milliliters per mole of reacted molecules). This last step can also be used to convert the volume change, ΔV_i, obtained with the TT method using Eq. 3 to molar reaction volumes.

The TT and MT methodologies have different goals. The TT method allows one to carry out titrations where either the ApoMb concentration or the pH is changed, and the response of the rate constants and the volume changes are followed. This method gives a rather good estimate of rate constants and volume changes. The MT method is used to determine the enthalpic changes associated with each transient and the activation energy for those processes whose rate constant is within the detection range of time-resolved photoacoustics. In the MT method, the pH and the ApoMb concentration are held fixed. The determination of the structural volume changes is more precise using the MT method, because the value is obtained with a linear regression and not from a single measurement, as in the case of the TT method (see Eqs. 3 and 4).

Kinetic considerations

Under our experimental conditions, the concentration of photoreleased protons is below 1 μM (Viappiani et al., 1998a). Also, at all prepulse pH values above 3.5, the quantum yield for proton release is constant (Pelagatti et al., 1998), thus leading to the same change in concentration of free protons right after the end of the laser pulse. The caged proton we have used, *o*NBA, is characterized by an irreversible photochemistry, leading to a stable photoproduct, *o*-nitrosobenzoic acid, that cannot bind the released proton back. We therefore achieve a step increase of 1 μM in proton concentration independent of the starting pH. For instance, when the prepulse pH is 7.0, immediately after the laser pulse the pH of the solution becomes 6.0. In the absence of ApoMb or other buffering components, this change lasts hundreds of milliseconds (Viappiani et al., 1998b). On longer time scales, diffusion of protons out of the illuminated volume slowly re-equilibrates the pH.

The ground state protonation reactions induced by the laser pH jump are diagrammed in Scheme 1, where photoreleased protons can react with different binding sites on the protein (indicated as P_i) with rate constants k_{i+} (binding) and k_{i-} (dissociation).

$$oNBA + h\nu \rightarrow NBA^- + H^+$$

$$H^+ + P_i^- \underset{k_{i-}}{\overset{k_{i+}}{\rightleftharpoons}} HP$$

$$P_F \underset{k_F}{\overset{k_U}{\rightleftharpoons}} P_U$$

(Scheme 1)

The protonation reactions can be treated as pseudo-first order reactions, because the concentration of the acceptor sites ($([P_i^-] > 10 > 10$ μM) is always greatly in excess of the photoreleased protons. The resulting kinetics can be described by a sum of exponential decay functions. Following the diffusion-mediated binding of protons, the protein may undergo structural changes, adding other first-order equilibria to the kinetic scheme.

RESULTS

In our experiments the concentration of free protons is rapidly increased by flashing the solution containing the caged proton *o*NBA (Viappiani et al., 1998a,b; Pelagatti et al., 1998; Bonetti et al., 1997), ApoMb, and 200 mM GuHCl. We have conducted experiments in which we have measured the response of the protein to the proton concentration jump as a function of the prepulse pH, concentration of the protein, and temperature of the solution.

When the solution contained only *o*NBA, only a fast, subresolution contraction (lifetime below a few nanoseconds) was detectable at all prepulse pH values (Bonetti et al., 1997; Pelagatti et al., 1998). This contraction is associated with solvation of both photoreleased proton and ni-

trosobenzoate anion. When the solution also contained ApoMb, additional kinetic events were detected, associated with the protonation of peptide residues. In particular, when the prepulse pH is near neutrality, we induce the unfolding reaction N→I. These events are described below.

pH titrations with the TT method

The prepulse pH values of aqueous solutions of ApoMb and *o*NBA were adjusted over a range of 4.5 to 7.5. Pure volumetric signals were obtained for these samples at T = 1.79°C. Examples of the waveforms obtained are shown in Fig. 2, along with a reference waveform acquired at T = 5.0°C. The shape of the signal is strongly dependent on the prepulse pH and shows a fast contraction, more evident at the lower pH values, followed by a slower expansion. The signal becomes smaller and more structured around neutrality.

Deconvolution of the experimental waveforms indicates triexponential decays near neutrality and biexponential decays below pH 5.5. The analysis results were of a quality similar to that of previously published data (Bonetti et al., 1997; Losi and Viappiani, 1998). The structural volume changes recovered from these analyses are reported in Fig. 3. A fast, subresolution (lifetime below a few nanoseconds) contraction is detectable at all investigated pH values. This component is associated with release and solvation of the proton (Viappiani et al., 1998a; Pelagatti et al., 1998; Bonetti et al., 1997; Losi and Viappiani, 1998). An expansion (lifetime in the hundreds of nanoseconds) is also present at all pH values, whereas a contraction occurring over microseconds is detectable only at pH values above 5.5.

As shown in Fig. 4, the two slower transients have lifetimes that increase on lowering the pH of the solution. This observation is consistent with an ionic equilibrium in which the concentration of a reacting species is decreased as the pH is lowered.

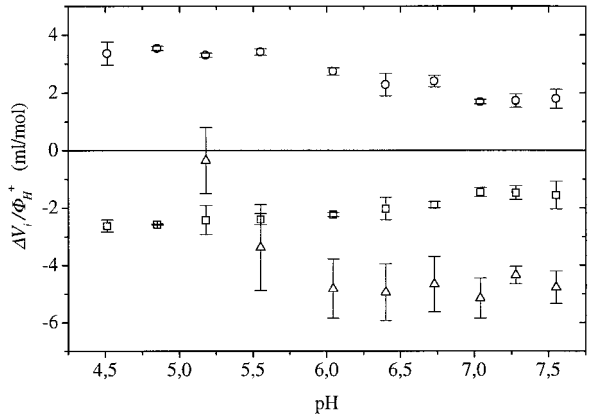

FIGURE 3 Prepulse pH dependence of structural volume changes of an aqueous solution of *o*NBA and ApoMb determined by deconvolution of volumetric signals acquired at T = 1.79°C. Absorbance of the solution (due only to *o*NBA) at 355 nm was 0.4 (1 cm path length), [ApoMb] = 80 μM, [GuHCl] = 0.2 M. The structural volume changes have been determined by means of Eq. 3 and dividing the values by the deprotonation quantum yield 0.4 (George and Scaiano, 1980; Viappiani et al., 1998a; Pelagatti et al., 1998). Plots report $\Delta V_1/\Phi_H^+$ (□), $\Delta V_2/\Phi_H^+$ (○), and $\Delta V_3/\Phi_H^+$ (△).

In addition, the apparent lifetime of transient 3, as reported in Fig. 4, reaches a plateau near neutrality. The sharp increase in the lifetime of this transient below pH 6.0 is paralleled by the drop in the magnitude of $\Delta V_3/\Phi_H^+$. At pH < 5.5, the combination of small amplitude and very long lifetime makes this component undetectable.

The decrease in magnitude of $\Delta V_1/\Phi_H^+$ and $\Delta V_2/\Phi_H^+$ apparent in Fig. 3 would seem to indicate some sort of transition centered near pH 6.2. However, this behavior is likely artifactual, the result of a cross-correlation (Bevington,

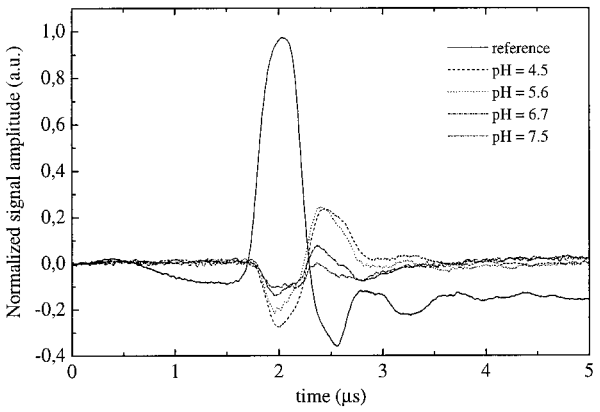

FIGURE 2 Volumetric signals of an aqueous solution of *o*NBA and ApoMb at T = 1.79°C at different prepulse pH values. Absorbance of the solution (due only to *o*NBA) at 355 nm was 0.4 (1 cm path length), [ApoMb] = 80 μM, [GuHCl] = 0.2 M. The reference compound (BP) signal was acquired at 5.0°C.

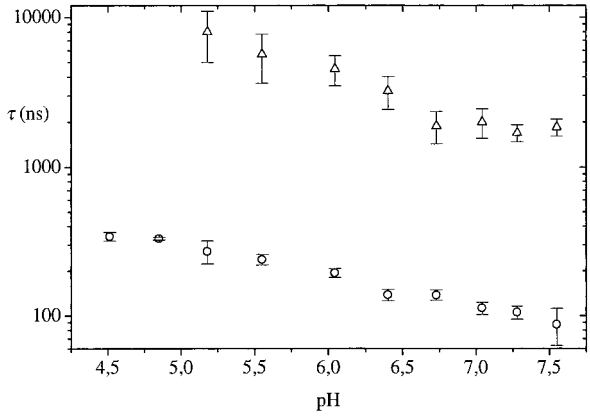

FIGURE 4 Prepulse pH dependence of lifetimes of the structural volume changes of an aqueous solution of *o*NBA and ApoMb determined by deconvolution of volumetric signals acquired at T = 1.79°C. Absorbance of the solution (due only to *o*NBA) at 355 nm was 0.4 (1 cm path length), [ApoMb] = 80 μM, [GuHCl] = 0.2 M. Plots report τ_2 (○) and τ_3 (△).

1969) of the fitting parameters (φ_1, φ_2, and τ_2), which, when τ_2 drops below 150 ns, may affect the ability of the deconvolution analysis to properly resolve the two faster decays (Bonetti et al., 1997).

The protonation of carboxylates on a protein is known to lead to an expansion of the solution (Rasper and Kauzmann, 1962a,b; VanEldick et al., 1989). One expects such an expansion because the protonation of the $-COO^-$ on Glu or Asp residues neutralizes two net charges, eliminating strong electrostrictive effects and affecting specific interactions around the carboxylates (e.g., hydrogen bonds or salt bridges). The sign of the volume change and the pH dependence of the lifetime (increasing lifetime with decreasing pH) are consistent with the assignment of transient 2 as being due to the neutralization of carboxylates on the protein.

The contraction associated with the longer-lived transient suggests the involvement of an initially neutral species on ApoMb that, when protonated, induces a contraction, possibly including effects due to increased electrostriction. The sign of the volume change and the disappearance of the transient at pH below 5.5 is compatible with protonation of His residues (Rasper and Kauzmann, 1962a,b; VanEldick et al., 1989), whose pK_a is in this pH region (Cocco et al., 1992). The disappearance of this transient occurs at the same pH at which the compact acid intermediate is formed (*vide supra*). Decay component 3, thus, likely derives from a process induced by proton binding to histidine residues on the ApoMb.

The plateau in τ_3 at neutrality in Fig. 4, corresponds to a limiting rate of $k_{3p} = 0.52 \pm 0.08\ 10^6\ s^{-1}$ (see Table 1).

ApoMb concentration titration with the TT method

To determine the bimolecular rate constants for the two transients evidenced in the pH-dependent experiments, we measured the response of the apparent rate constants to the concentration of ApoMb at two different values of pH. We chose pH values above 7.0 and below 4.5, the apparent pK_a of the N→I transition.

A triexponential decay was found at pH 7.0 at ApoMb concentrations above 25 μM. The fast contraction due to proton solvation (component 1) is followed by an expansion (component 2). As shown in Fig. 5 *A*, at pH 7.0 the rate constant ($k_2 = 1/\tau_2$) of this expansion increases in a linear manner on increasing the concentration of ApoMb. The bimolecular rate constant k_{2b} obtained from the slope of the linear plot of k_2 vs. [ApoMb] (Fig. 5 *A*) is reported in Table 1.

A further contraction (component 3) occurs in the microsecond range. A plot of $k_3 = 1/\tau_3$ vs. [ApoMb] (Fig. 5 *B*) is nonlinear and shows an increase in k_3 in the low concentration range, reaching a plateau of $k_{3p} = (0.68 \pm 0.06) \times 10^6\ s^{-1}$ at higher concentrations (Table 1). This value is essentially identical to the plateau value obtained in the pH-dependent experiment. We presume that the saturation

TABLE 1 Parameters from concentration-dependent experiments for ApoMb

Bimolecular binding rate constants ($10^{10}\ M^{-1}\ s^{-1}$)	pH = 4.5	pH = 7.0
k_{2b}	4.1 ± 0.1	12.5 ± 0.2
k_{3b}	—	0.77 ± 0.03
Limiting rate constants ($10^6\ s^{-1}$)†		
k_{3p} (estimated from data of Figure 4)	—	0.52 ± 0.08
k_{3p} (estimated from data of Figure 5B)	—	0.68 ± 0.06
Reaction volumes (ml/mol)‡		
$\Delta V_{R,1}$	−2.51 ± 0.11	−2.45 ± 0.13
$\Delta V_{R,2}$	3.31 ± 0.19	3.7 ± 0.16
$\Delta V_{R,3}$	—	−62 ± 11

*Bimolecular rate constants k_{2b} and k_{3b} are obtained from the linear plots of k_2 and k_3 vs [ApoMb], Figs. 5 and 6, respectively. For k_3, only the low concentration data were used.

†Limiting rate constants were estimated from the plateau regions of τ_3 and k_3 in Figs. 4 and 5 *B*, respectively.

‡Reaction volumes are estimated as $\Delta V_{R,i} = \Delta V_i/(\Phi_H^+ \eta_i)$, where ΔV_i is determined according to Eq. 3, $\Phi_H^+ = 0.4$, $\eta_2 = 0.942$, and $\eta_3 = 0.058$ (see text, Eq. 5). For transient 1 we have $\Delta V_{R,1} = \Delta V_1/\Phi_H^+$ (i.e., $\eta_1 = 1.0$).

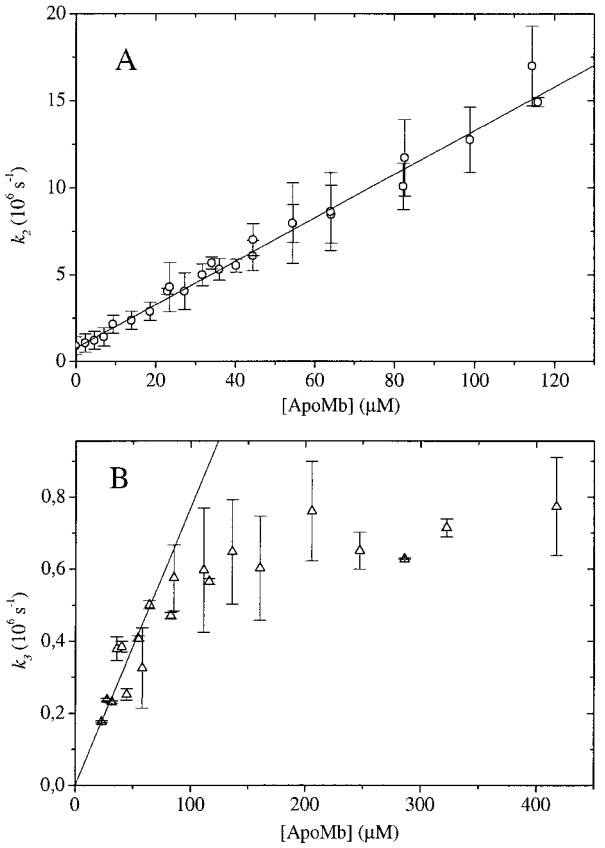

FIGURE 5 Rate constants ($k_i = 1/\tau_i$) for the transients detected in an aqueous solution of *o*NBA and ApoMb at pH 7.0, as a function of [ApoMb]. Absorbance of the solution (due only to *o*NBA) at 355 nm was 0.4 (1 cm path length), T = 1.79°C, [GuHCl] = 0.2 M. (*A*) Rate constant for the expansion. (*B*) Rate constant for the contraction. The bimolecular binding rate constants obtained assuming pseudo first-order kinetics are reported in Table 1.

of k_3, corresponding to a lifetime of about 1.5 μs, results from a sequential reaction after the protonation of the imidazole ring, constituting a rate-limiting step. The two steps, which in principle would give rise to more complex kinetics, cannot be separated due to limitations in the experimental resolution and are integrated into a single exponential relaxation. The slope obtained from the low concentration range gives an estimate of the rate constant, k_{3b}, for the diffusion-mediated proton binding process and is reported in Table 1.

As indicated in Table 1, the value of $\Delta V_1/\Phi_H^+$ gives directly the molar reaction volume $\Delta V_{R,1}$ for the rapid deprotonation of *o*NBA. If reactions 2 and 3 are interpreted as parallel processes due to the protonation of carboxylates (transient 2) and histidines (transient 3), respectively, the volume changes must be corrected not only for Φ_H^+ but also for the efficiency of each process in order to obtain reaction volumes. Efficiencies for transients 2 and 3, η_2 and η_3, can be estimated from the bimolecular rate constants of these competitive protonation reactions. In the absence of other competitive reactions, these efficiencies can be written (Laidler, 1987) as:

$$\eta_2 = \frac{k_{2b}}{k_{2b} + k_{3b}}$$
$$\eta_3 = \frac{k_{3b}}{k_{2b} + k_{3b}} \quad (5)$$

Using the rate constants k_{2b} and k_{3b} reported in Table 1 we obtain $\eta_2 = 0.942$ and $\eta_3 = 0.058$. In order to obtain the reaction volume for each transient ($\Delta V_{R,1}$ and $\Delta V_{R,2}$), $\Delta V_1/\Phi_H^+$ and $\Delta V_2/\Phi_H^+$ must be divided by the relative efficiencies η_2 and η_3. Reaction volumes thus calculated are reported in Table 1.

At prepulse pH 4.5, the protein is mainly in state I. In this case, deconvolution of the experimental waveforms is best obtained with a biexponential decay, in which the fast contraction due to the solvation of the newly produced charges is followed by an expansion in the hundreds of nanoseconds, presumably due to the protonation of carboxylates on ApoMb. The plot of the rate constant against [ApoMb] is reported in Fig. 6 and the slope of the linear regression is reported in Table 1. The calculated reaction volumes for both proton release and protonation of carboxylates are independent of pH (4.5 and 7.0; Table 1).

MT experiments

MT experiments in the range of 2 to 30°C were conducted at two pH values, one above and one below the N→I transition, in order to determine enthalpic changes associated with each transient and an independent estimate of the structural volume changes (Eq. 4). Also, the temperature dependence of the lifetime provides information on the activation energy for each process whose rate constant falls within the experimental resolution range.

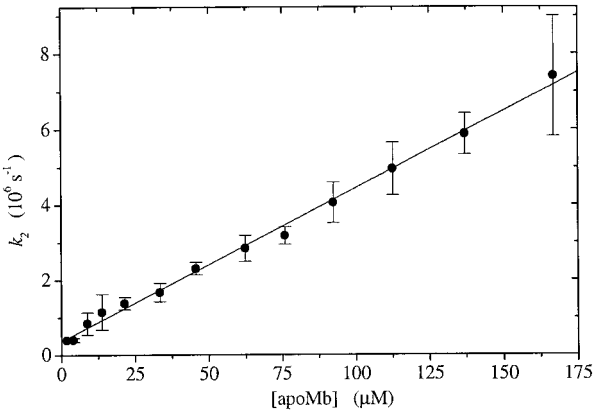

FIGURE 6 Rate constants ($k_2 = 1/\tau_2$) for the expansion detected in an aqueous solution of *o*NBA and ApoMb at pH 4.5, as a function of [ApoMb]. Absorbance of the solution (due only to *o*NBA) at 355 nm was 0.4 (1 cm path length), T = 1.79°C, [GuHCl] = 0.2 M. The bimolecular binding rate constant obtained assuming pseudo first-order kinetics is reported in Table 1.

The MT studies indicate the same number of exponentials as were observed in the pH- and concentration-dependent experiments. Fig. 7, *A* and *B*, shows plots of the amplitude results in accordance with Eq. 4 for the results obtained at pH 7.0 and 4.5, respectively. The parameters obtained by linear fits to the data series (Q_i and $\Delta V_i = \Phi_i \Delta V_{R,i}$) are summarized in Table 2. The molar volume changes obtained compare very favorably with those from the TT experiments (Table 1).

Arrhenius plots for the rate constants of each decay are reported in Fig. 8, and the pre-exponential factors and activation energies obtained from the linear fits to the data as shown are reported in Table 2.

The overall results are summarized in Scheme 2 and are discussed below.

DISCUSSION

Protonation of carboxylates

When acid is added to an aqueous solution of a protein around and below neutrality, the principal reaction is protonation of carboxylates. For small carboxylic acids the volume change expected is between 10 and 14 ml/mol, depending on the nature of the group attached to the carboxylate (VanEldick et al., 1989; Rasper and Kauzmann, 1962b). If positively charged groups exist close to the carboxylate, then the volume increase will be smaller, 6 or 7 ml/mol (VanEldick et al., 1989). In proteins the volume change is about 11 ml/mol, but in some cases smaller values can be observed, possibly related to the proximity of positively charged residues (Rasper and Kauzmann, 1962a).

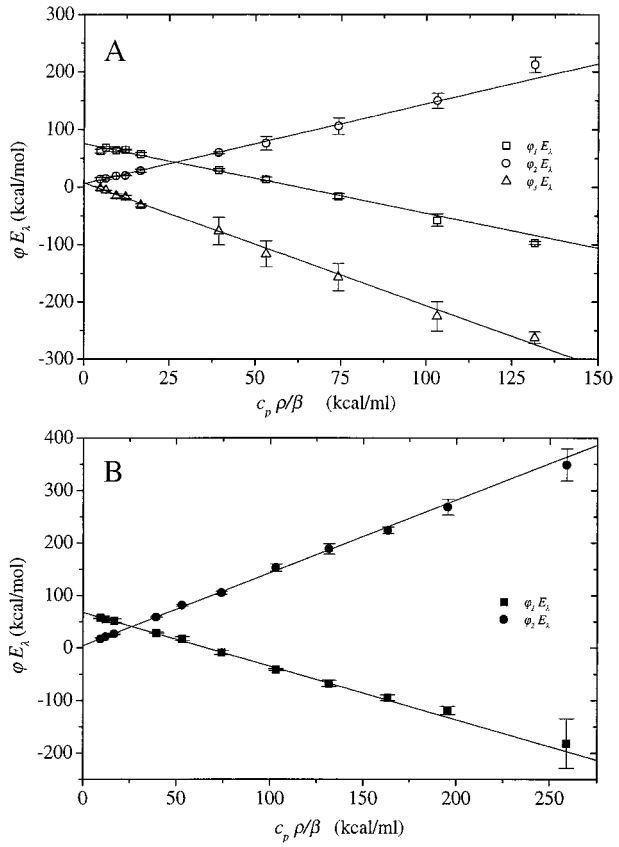

FIGURE 7 Energy content of the transient species ($\varphi_i E_\lambda$) as a function of the thermoelastic parameter $C_p\rho/\beta$ of the solution. (*A*) pH 7.0, [ApoMb] = 50 μM, [GuHCl] = 0.2 M; (*B*) pH 4.5, [ApoMb] = 58 μM [GuHCl] = 0.2 M. For both samples, the absorbance of the solution (due only to *o*NBA) at 355 nm was 0.4 (1 cm path length). Symbols are explained in the figure. The results of the linear interpolation for each transient are reported in Table 2.

The reaction volumes determined by the MT and TT methods reported in Tables 1 and 2 show very good consistency. The smaller than expected volume change assigned to carboxylate protonation (about 3.4 ml/mol) probably reflects the influence of lysine and arginine groups, which are completely protonated around and below neutrality.

TABLE 2 Parameters from temperature dependent experiments for ApoMb

Enthalpy changes (kcal/mol)	pH = 4.5	pH = 7.0
Q_1	70 ± 1	81 ± 2
Q_2	4 ± 1	2 ± 2
Q_3	—	8 ± 1
Reaction volumes (ml/mol)		
$\Delta V_{R,1}$	−2.3 ± 0.1	−2.73 ± 0.07
$\Delta V_{R,2}$	3.06 ± 0.05	3.4 ± 0.2
$\Delta V_{R,3}$	—	−82 ± 3
Activation energy (kcal/mol)		
E_{a2}	9.1 ± 0.8	9.2 ± 0.9
E_{a3}	—	16.2 ± 0.9
Pre-exponential factors (s^{-1})		
A_2	4.60×10^{13}	7.68×10^{13}
A_3	—	2.74×10^{18}

See notes to Table 1 for explanation of symbols.

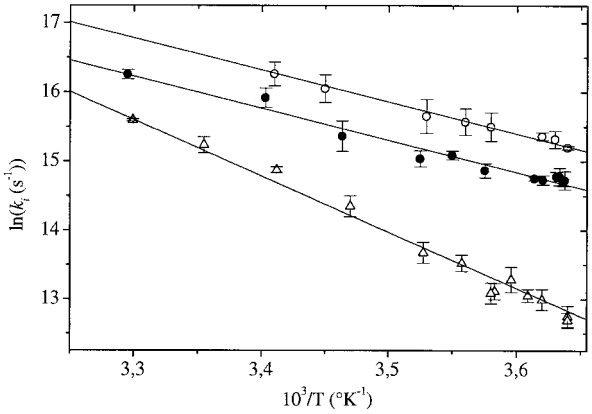

FIGURE 8 Arrhenius plots for the protonation reactions of carboxylates at pH 7.0 (○) and 4.5 (●) and of histidines at pH 7.0 (△). Results of the interpolation with straight lines are reported in Table 2.

The reaction enthalpy for protonation of the acidic groups in apomyoglobin has been estimated to be 0.4 kcal/mol for α-carboxy (C-terminus) and γ-carboxy (Glu) and 1.1 kcal/mol for β-carboxy (Asp; Griko et al., 1988; Weast, 1968). Our estimates provide somewhat larger values at both pH 4.5 and pH 7.0; however, the large estimated error in our measurements precludes any precise comparison with the literature.

Our rate constants for protonation of carboxylates can be compared to values reported by Gutman in different proteins: $(2.5 \times 10^{10})M^{-1}\ s^{-1}$ for BSA and RNase, and $(1.2 \times 10^{10})M^{-1}\ s^{-1}$ for lysozyme (Gutman and Nachliel, 1990). In Table 1 we present values of k_{2b} measured by means of a linear plot of the apparent rate constant k_2 versus the concentration of the protein, rather than versus the concentration of protonatable sites. At neutrality the total number of protonatable sites per molecule is 22, 11 of which are carboxylates, whereas at pH 4.5 the total number is 10, with possibly only one His not protonated (Cocco et al., 1992; Griko et al., 1988). If we assume for the bimolecular rate an average literature value of $k_{2av} = (1.85 \times 10^{10})M^{-1}\ s^{-1}$ (Gutman and Nachliel, 1990), we can estimate the average number of reacting carboxylates as the ratio between k_{2b} and k_{2av}. The effective numbers of sites per molecule we get are 2.2 at pH 4.5 and 5.7 at pH 7.0.

Protonation of histidines and early structural changes in the N→I transition

Protonation of the imidazole ring of histidine free in solution is known to be accompanied by a small contraction of about −1 ml/mol (VanEldick et al., 1989). Our observed transient 3 shows an appropriate pH response and has the correct sign for protonation of a His residue. However, the

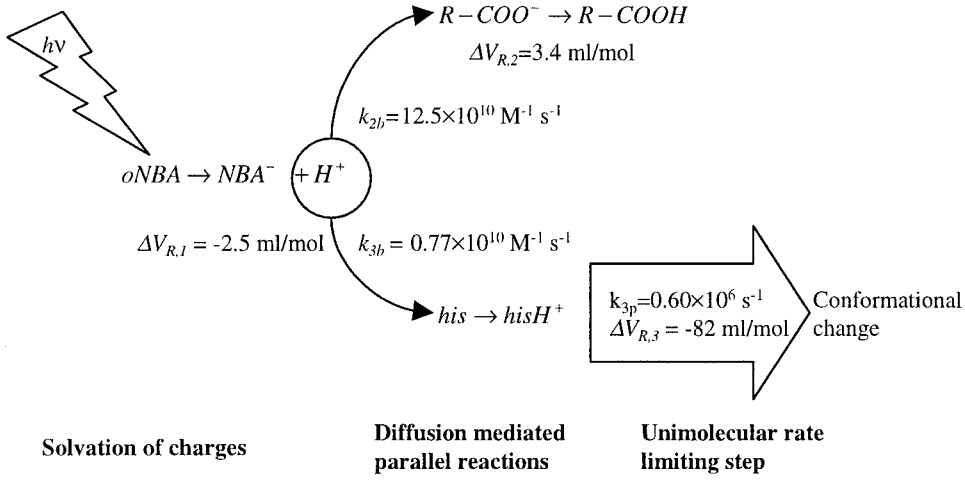

Scheme 2.

recovered reaction volume, $\Delta V_{R,3}$ (Table 1 using the TT method and Table 2 using the more accurate MT method; Gensch and Braslavsky, 1997; Losi and Viappiani, 1998) is much too large to be accounted for on the basis of simple protonation of the imidazole ring. This discrepancy can be explained if we assume that protonation of His induces a unimolecular structural rearrangement, which becomes rate-limiting at high ApoMb concentration. The observed large volume change can be assigned to this structural rearrangement.

Although the contribution of the protonation process itself cannot be observed, the limiting behavior of the structural change at very low [ApoMb] should give a reasonable estimate of the diffusion-mediated protonation kinetics. The slope in the low concentration range of Fig. 5 *B* provides a bimolecular rate constant of $(0.77 \pm 0.03) \times 10^{10}\ M^{-1}\ s^{-1}$, somewhat larger than the literature value of $(0.5 \times 10^{10}) M^{-1}\ s^{-1}$ in RNase and for His64 of ApoMb (Gutman and Nachliel, 1990). The ratio between our result and the literature value provides an estimate of 1.5 for the number of His residues involved in this reaction. This result is consistent with the equilibrium data in Fig. 1, which indicate 1.4 and 1.9 protons are bound in the N→I transition from the CD and fluorescence data, respectively, and from Barrick et al. (1994).

The pH region in which the transient occurs is compatible with protonation of His48 ($pK_a = 5.2$), His113 ($pK_a = 5.5$), His116 ($pK_a = 6.6$), His119 ($pK_a = 5.3$–5.8), and His24, which has a lower pK_a (< 4.8; Cocco et al., 1992). However, His48, His113, and His116 are all solvent-exposed (Barrick et al., 1994) and no large structural effects are expected upon binding of a proton. His119 and His24, on the other hand, have a very important role in stabilizing the native state of ApoMb. In the native form, His119 is hydrogen bonded to His24 (Dalvit and Wright, 1987; Cheng and Schoenborn, 1991) within the hydrophobic core of the protein, at the interface between the two subdomains (Cocco et al., 1992; Cocco and Lecomte, 1990) constituted by helices A, G, H and B, C, D, E (Hughson et al., 1990, 1991). Fig. 9 shows the location and the interaction between His24 and His119 at the interface between the two subdomains in native horse heart myoglobin (Protein Data Bank entry 1WLA). Hydrogen exchange studies indicate that the helices A, G, H are present in the ApoMb intermediate, I, whereas helices B through E are not (Hughson et al., 1990). Also, it has been suggested that the formation of the hydrogen bond between His24 and His119 may be a rate-limiting step in the refolding of I to the native state (Barrick et al., 1994). The refolding involves motions of large portions of the molecule and is expected to proceed through a series of

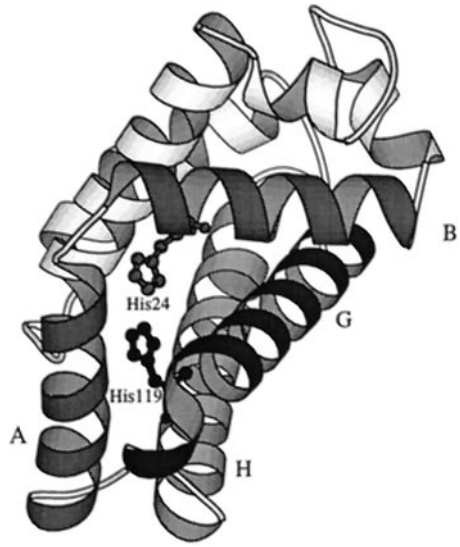

FIGURE 9 Location of His24 and His119 in native horse heart myoglobin (Protein Data Bank entry 1WLA).

events characterized by different rates, extending from microseconds to milliseconds.

The large contraction we measured above pH 5.5 is likely related to the protonation of His119/His24, the hydrogen-bonded histidine pair. This protonation would lead to the formation of a resonant structure (Barrick et al., 1994), where the positive charge is shared, and a partial disruption of the hydrogen bond between the two histidines. Weakening of the hydrogen bond could result in partial solvation of previously buried residues at the interface between helix B and the core AGH, contributing to the relatively large contraction of the solution (Chalikian, 1996). It is unlikely that the measured events reflect significant changes in the structure of the AGH core (Gilmanshin et al., 1997a; Eliezer et al., 1998). They may reflect partial unfolding of the BCDE structure, although some aspects of such a major change may be too slow to be detected in the experiments reported here.

This hypothesis is supported by the temperature dependence of the rate constant for the process, shown in Fig. 8. The protonation of carboxylates has an activation energy of about 9 kcal/mol regardless of the state of the protein (N or I). In contrast, the activation barrier for protonation of His119/His24 and the following structural rearrangement is about 16 kcal/mol, a relatively large value, indicating that this step is of key importance in stabilizing N with respect to I.

The enthalpy change for the protonation of His has been reported to be 6.9 kcal/mole (Weast, 1968). Our estimate of 8 kcal/mol is in agreement with this result. Even if the higher value is significant, it suggests that the subsequent changes giving rise to the large structural volume change make only a small contribution to the enthalpy. The structural volume changes appear therefore to be a more appropriate parameter for monitoring the peculiar structural transition induced by protonation of His199/His24 in ApoMb. They may better reflect the entropic contributions to the process which, in this system, are expected to play a major role. Entropic factors have been shown to correlate with structural volume changes in electron and proton transfer processes (Hepler, 1965; Borsarelli and Braslavsky, 1998).

The rate-limiting constant we have measured for the changes after protonation of His119/His24 is comparable to other rates recently measured in folding or unfolding studies. For instance, the rate constant for unfolding of a 16-amino acid hairpin was (0.17×10^6) s^{-1} (Muñoz et al., 1997), and the limiting rate due to the molecular chain diffusion for cytC was in the 10^6 s^{-1} range (Jones et al., 1993). It seems therefore that even in the presence of substantial structural rearrangements, limiting rates for specific events can be found in the 10^6 s^{-1} range. The meaning of such ultrafast events within the protein folding pathway has been recently discussed in relation to essentially non-specific solvation processes (Sosnick et al., 1997).

CONCLUSIONS

Changes in volume represent a sensitive tool for monitoring structural events in which the solvation of the protein is altered and constitute a prompt, intrinsic probe of the system under investigation. Despite the relatively narrow time range accessible by time-resolved photoacoustics (20 ns − 10 μs), we have shown that a great deal of information can be obtained on the primary events accompanying the acid perturbation, including the proton binding process and the early conformational rearrangements. Extension of the laser-induced pH jump technique to longer time scales may allow a more detailed study of the overall time course of the structural changes, including events involving movements of large portions of the macromolecule.

S. A., A. V., and C. V. acknowledge Istituto Nazionale per la Fisica della Materia (Progetto Speciale di Sezione B) and CNR for financial support. Fig. 9 was prepared using Molscript with the help of Eugenia Polverini.

REFERENCES

Ballew, R. M., J. Sabelko, and M. Gruebele. 1996a. Direct observation of fast protein folding: the initial collapse of apomyoglobin. *Proc. Natl. Acad. Sci. USA.* 93:5759–5764.

Ballew, R. M., J. Sabelko, and M. Gruebele. 1996b. Observation of distinct nanosecond and microsecond protein folding events. *Nat. Struct. Biol.* 3:923–926.

Barrick, D., and R. L. Baldwin. 1993. The molten globule intermediate of apomyoglobin and the process of protein folding. *Protein Sci.* 2:869–876.

Barrick, D., F. M. Hughson, and R. Baldwin. 1994. Molecular mechanism of acid denaturation of apomyoglobin: the role of hystidine residues in the partial unfolding of apomyoglobin. *J. Mol. Biol.* 237:588–601.

Bevington, P. R. 1969. Data reduction and error analysis for the physical sciences. McGraw-Hill, New York.

Bonetti, G., A. Vecli, and C. Viappiani. 1997. Reaction volume of water formation detected by time resolved photoacoustics: photoinduced proton transfer between o-nitrobenzaldehyde and hydroxyls in water. *Chem. Phys. Lett.* 269:268–273.

Borsarelli, C. D., and S. E. Braslavsky. 1998. Volume changes correlate with enthalpy changes during the photoinduced formation of the (MLCT)-M3 state of ruthenium (II) bipyridine cyano complexes in the presence of salts. A case of entropy-enthalpy compensation effect. *J. Phys. Chem. B.* 102:6231–6238.

Braslavsky, S. E., and G. E. Heibel. 1992. Time-resolved photothermal and photoacoustics methods applied to photoinduced processes in solution. *Chem. Rev.* 92:1381–1410.

Callis, J. B., W. W. Parson, and M. Gouterman. 1972. Fast changes of enthalpy and volume of flash excitation of *chromatium* chromatophores. *Biochim. Biophys Acta.* 267:348–362.

Chalikian, T. V. 1996. On volume changes accompanying conformational transitions of biopolymers. *Biopolymers.* 39:619–626.

Chan, C., Y. Hu, S. Takahashi, D. L. Rousseau, W. A. Eaton, and J. Hofrichter. 1997. Submillisecond protein folding kinetics studied by ultrarapid mixing. *Proc. Natl. Acad. Sci. USA.* 94:1779–1784.

Chen, Y., and M. D. Barkley. 1998. Toward understanding tryptophan fluorescence in proteins. *Biochemistry.* 37:9976–9982.

Cheng, X., and B. P. Schoenborn. 1991. Neutron diffraction study of carbonmonoxymyoglobin. *J. Mol. Biol.* 220:381–399.

Cocco, M., Y. H. Kao, A. Phillips, and J. T. J. Lecomte. 1992. Structural comparison of apomyoglobin and metaquomyoglobin: pH titration of histidines by NMR spectroscopy. *Biochemistry.* 31:6481–6491.

Cocco, M. J., and J. T. J. Lecomte. 1990. Characterization of hydrophobic cores in apomyoglobin: a proton NMR spectroscopy study. *Biochemistry.* 29:11067–11072.

Cocco, M. J., and J. T. J. Lecomte. 1994. The native state of apomyoglobin described by proton NMR spectroscopy: interaction with the paramagnetic probe HyTEMPO and fluorescent dye ANS. *Protein Sci.* 3:267–281.

Dalvit, C., and P. E. Wright. 1987. Assignment of resonances in the ^{1}H nuclear magnetic resonance spectrum of the carbon monoxide complex of sperm whale myoglobin by phase-sensitive two dimensional techniques. *J. Mol. Biol.* 194:313–327.

Eliezer, D., P. A. Jennings, P. E. Wright, S. Doniach, K. O. Hodgson, and H. Tsuruta. 1995. The radius of gyration of an apomyoglobin folding intermediate. *Science.* 270:487–488.

Eliezer, D., J. Yao, H. J. Dyson, and P. E. Wright. 1998. Structural and dynamic characterization of partially folded states of apomyoglobin and implications for protein folding. *Nat. Struct. Biol.* 5:148–155.

Gensch, T., and S. E. Braslavsky. 1997. Volume changes related to triplet formation of water-soluble porphyrins: a laser-induced optoacoustic spectroscopy (LIOAS) study. *J. Phys. Chem.* 101:101–108.

George, M. V., and J. C. Scaiano. 1980. Photochemistry of o-nitrobenzaldehyde and related studies. *J. Phys. Chem.* 84:492–495.

Gilmanshin, R., R. H. Callender, and R. B. Dyer. 1998. The core of apomyoglobin E-form folds at the diffusion limit. *Nat. Struct. Biol.* 5:363–365.

Gilmanshin, R., R. B. Dyer, and R. H. Callender. 1997a. Structural heterogeneity of the various forms of apomyoglobin: implications for protein folding. *Protein Sci.* 6:2134–2142.

Gilmanshin, R., S. Williams, R. H. Callender, W. H. Woodruff, and R. B. Dyer. 1997b. Fast events in protein folding: relaxation dynamics of secondary structure in native apomyoglobin. *Proc. Natl. Acad. Sci. USA.* 94:3709–3713.

Griko, Y. V., P. L. Privalov, and S. Y. Venyaminov. 1988. Thermodynamic study of apomyoglobin structure. *J. Mol. Biol.* 202:127–138.

Gutman, M., and E. Nachliel. 1990. The dynamic aspects of proton transfer processes. *Biochim. Biophys Acta.* 1015:391–414.

Harrison, S. C., and R. Blout. 1965. Reversible conformational changes of myoglobin and apomyoglobin. *J. Biol. Chem.* 240:299–303.

Hepler, L. G. 1965. Entropy and volume changes on ionization of aqueous acids. *J. Phys. Chem.* 69:965.

Hughson, F. M., D. Barrick, and R. L. Baldwin. 1991. Probing the stability of a partly folded apomyoglobin intermediate by site-directed mutagenesis. *Biochemistry.* 30:4113–4118.

Hughson, F. M., P. E. Wright, and R. L. Baldwin. 1990. Structural characterization of a partly folded apomyoglobin intermediate. *Science.* 249:1544–1548.

Jennings, P. A., and P. E. Wright. 1993. Formation of a molten globule intermediate early in the kinetic folding pathway of apomyoglobin. *Science.* 262:892–896.

Johnson, R. S., and K. A. Walsh. 1994. Mass spectrometric measurement of protein amide hydrogen exchange rates of apo- and holo- myoglobin. *Protein Sci.* 3:2411–2418.

Jones, C. M., E. R. Henry, Y. Hu, C. Chan, S. D. Luck, A. Bhuyan, H. Roder, J. Hofrichter, and W. A. Eaton. 1993. Fast events in protein folding initiated by nanosecond laser photolysis. *Proc. Natl. Acad. Sci. USA.* 90:11860–11864.

Laidler, K. J. 1987. Chemical Kinetics. HarperCollins Publishers, New York.

Losi, A., and C. Viappiani. 1998. Reaction volume and rate constants for the excited state proton transfer in aqueous solutions of naphthols. *Chem. Phys. Lett.* 289:500–506.

Muñoz, V., P. A. Thompson, J. Hofrichter, and W. A. Eaton. 1997. Folding dynamics and mechanism of β-hairpin formation. *Nature.* 390:196–199.

Pelagatti, P., M. Carcelli, and C. Viappiani. 1998. Determination of the pKa of the aci-nitro intermediate in o-nitrobenzyl systems. *Israel J. Chem.* 38:213–221.

Peters, K. S., and G. J. Snyder. 1988. Time-resolved photoacoustic calorimetry: probing the energetics and dynamics of fast chemical and biochemical reactions. *Science.* 241:1053–1057.

Phillips, C. M., Y. Mizutani, and R. M. Hochstrasser. 1995. Ultrafast thermally induced unfolding of RNase A. *Proc. Natl. Acad. Sci. USA.* 92:7292–7296.

Privalov, P. L. 1996. Intermediate states in protein folding. *J. Mol. Biol.* 258:707–725.

Ramachandra Shastry, M. C., S. D. Luck, and H. Roder. 1998. A continuous-flow capillary mixing method to monitor reactions on the microsecond time scale. *Biophys. J.* 74:2714–2721.

Rasper, J., and W. Kauzmann. 1962a. Volume changes in protein reactions. I. Ionization reactions of proteins. *J. Am. Chem. Soc.* 84:1771–1777.

Rasper, J., and W. Kauzmann. 1962b. Volume changes in protein reactions. II. Comparison of ionization reactions in proteins and small molecules. *J. Am. Chem. Soc.* 84:1777–1788.

Rossi Fanelli, A., E. Antonini, and A. Caputo. 1958. *Biochim. Biophys Acta.* 30:608–615.

Rudzki, J. E., J. L. Goodman, and K. S. Peters. 1985. Simultaneous determination of photoreaction dynamics and energetics using pulsed, time-resolved photoacoustic calorimetry. *J. Am. Chem. Soc.* 107: 7849–7854.

Small, J. R. 1992. Deconvolution analysis for pulsed-laser photoacoustics. *In* Numerical Computer Methods. L. Brand and M. L. Johnson, editors. Academic Press, San Diego. 505–521.

Small, J. R., and E. Kurian. 1995. Volumetric photoacoustics: listening to more than just heat. *Spectroscopy.* 10:27–33.

Small, J. R., L. J. Libertini, and E. W. Small. 1992. Analysis of photoacoustic waveforms using the nonlinear least squares method. *Biophys. Chem.* 42:24–48.

Sosnick, T. R., M. D. Shtilerman, L. Mayne, and S. W. Englander. 1997. Ultrafast signals in protein folding and the polypeptide contracted state. *Proc. Natl. Acad. Sci. USA.* 94:8545–8550.

Thompson, P. A., W. A. Eaton, and J. Hofrichter. 1997. Laser temperature jump study of the helix-coil kinetics of an alanine peptide interpreted with a 'kinetic zipper' model. *Biochemistry.* 36:9200–9210.

VanEldick, R., T. Asano, and W. J. Le Noble. 1989. Activation and reaction volumes in solution. *2. Chem. Rev.* 89:549–688.

Viappiani, C., S. Abbruzzetti, J. R. Small, L. J. Libertini, and E. W. Small. 1998a. An experimental methodology for measuring volume changes in proton transfer reactions in aqueous solutions. *Biophys. Chem.* 73: 13–22.

Viappiani, C., G. Bonetti, M. Carcelli, F. Ferrari, and A. Sternieri. 1998b. Study of proton transfer processes in solution using the laser induced pH-jump: a new experimental setup and an improved data analysis based on genetic algorithms. *Rev. Sci. Instrum.* 69:270–276.

Waltho, J. P., V. A. Feher, G. Merutka, H. J. Dyson, and P. E. Wright. 1993. Peptide models of protein folding initiation sites. 1. Secondary structure formation by peptides corresponding to the G-helix and H-helix of myoglobin. *Biochemistry.* 32:6337–6347.

Weast, R. C. 1968. CRC Handbook of Biochemistry. CRC Press, Boca Raton, FL.

Weast, R. C. 1971. CRC Handbook of Chemistry and Physics. CRC Press, Boca Raton, FL.

Williams, S., T. P. Causgrove, R. Gilmanshin, K. S. Fang, R. H. Callender, W. H. Woodruff, and R. B. Dyer. 1996. Fast events in protein folding: helix melting and formation in a small peptide. *Biochemistry.* 35: 691–697.